Cement and Concrete Research 40 (2010) 271–283

Contents lists available at ScienceDirect

Cement and Concrete Research

journal homepage: http://ees.elsevier.com/CEMCON/default.asp

About microcracking due to leaching in cementitious composites: X-ray microtomography description and numerical approach

Thomas Rougelot [a], Nicolas Burlion [a,*], Dominique Bernard [b], Frédéric Skoczylas [c]

[a] Laboratoire de Mécanique de Lille, UMR CNRS 8107, Université Lille1, Polytech'Lille, Cité Scientifique, 59650 Villeneuve d'Ascq, France
[b] Institut de Chimie de la Matière Condensée de Bordeaux, ICMCB-CNRS-Université de Bordeaux, UPR CNRS 9048, 87 Av. du Dr A. Schweitzer, 33608 Pessac, France
[c] Laboratoire de Mécanique de Lille, UMR CNRS 8107, Ecole Centrale de Lille, Cité Scientifique, 59650 Villeneuve d'Ascq, France

ARTICLE INFO

Article history:
Received 23 January 2009
Accepted 24 September 2009

Keywords:
Cementitious composites
Endogenous and decalcification shrinkages
Leaching
Microcracking
X-ray computed microtomography

ABSTRACT

Chemical shock of cement based materials leads to significant degradation of their physical properties. A typical scenario is a calcium leaching due to water (water with very low pH compared with that of pore fluid). The main objective of this paper is to evaluate the evolution of microstructure induced by leaching of a cementitious composite using synchrotron X-ray micro tomography, mainly from an experimental point of view. In this particular case, it was possible to identify cracking induced by leaching. After a description of the degradation mechanism and the X-ray synchrotron microtomographic analysis, numerical simulations are performed in order to show that cracking is induced by an initial pre-stressing of the composite, coupled with decalcification shrinkage and dramatic decrease in tensile strength during leaching. X-ray microtomography analysis allowed to make evidence of an induced microcracking in cementitious material submitted to leaching.

1. Introduction

Mortars and concretes are non-homogeneous materials whose macroscopic properties depend on their local characteristics. For instance, their mechanical properties and permeability are intimately related to the microstructure. Therefore, it is of importance to link the local and the macroscopic scale to study and model the mechanical behaviour and the transport properties of cementitious materials. This requires the knowledge of the 3D micro-geometry and its evolution. To visualize this microstructure, various innovative techniques are in development as, for example, acoustic emission analysis, infrared thermography or X-ray computed micro tomography (XCMT).

Synchrotron XCMT finds applications in the study of sample microstructure without damaging it. The principle, similar to the medical scanner, consists of acquiring digital images of the material's X-ray absorption. These acquisitions are undertaken at various angles: a three-dimensional image is then obtained by numerical reconstruction from the set of 2D-images.

Concrete leaching is often the result of a fluid attack (pure water or water with very low pH compared to that of the pore fluid) that leads to the hydrolysis of cement paste hydrates, an important increase in porosity [1–3] and important decrease of mechanical properties [2,4–9]: existing models often use a damage behaviour in order to capture the main mechanical characteristic of the leached material [10–13]. Using synchrotron XCMT as a non-destructive characterization method and performing the accelerated leaching with an ammonium nitrate solution, it is possible to carry out the microtomographic analysis on the same specimen during the leaching process. It is then possible to determine the degradation kinetics, the leaching front position and the porosity increase without interfering with the material [14]. It is also possible to show that a cracking occurs in the concrete material during such a process. This cracking is due to tensile strength decrease induced by leaching. The cementitious materials containing aggregates (glass spheres in the present case) are auto-stressed materials [15] as the endogenous shrinkage of the cementing matrix causes a contraction around aggregates, that can be enhanced by decalcification shrinkage [16]. This contraction is important but leads generally to stress values lower than tensile strength. On the other hand, in the particular case of leaching, a drastic decrease in matrix tensile strength is observed with chemical attack. Microcracking will occur mainly around the gravels, what results in notably weaker material mechanical capacities. In order to confirm or not these hypotheses, a numerical study was performed. Modelling of coupled leaching-cracking (hydro-chemical coupling) is of interest, mainly for long-term behaviour of concrete in nuclear waste disposals, and the research is very intensive in this domain. The selected model, chosen to highlight the preferential areas of cracks nucleation, is conducted by the use of a finite element code in nonlinear mechanics. It is, on purpose, resolutely simple, and constitutes a first numerical approach of the samples mechanical behaviour during leaching.

In the first part, mortar degradation mechanism is described, and the principles of synchrotron XCMT presented. In the second part, a numerical simulation of mortar leaching is proposed and results

* Corresponding author.
E-mail address: nicolas.burlion@polytech-lille.fr (N. Burlion).

0008-8846/$ – see front matter © 2009 Elsevier Ltd. All rights reserved.
doi:10.1016/j.cemconres.2009.09.021

obtained demonstrate that the hypotheses made on the causes of concrete cracking during leaching are valid.

2. Experimental device and measurements

2.1. XCMT: principles

XCMT is a non destructive method which, for many materials [17,18], and for instance for cement based materials [19–25], leads to a 3D view representation of the sample without damaging it. The most used technique is transmission tomography, where a detector measures the resulting intensity of a known unidirectional (x-axis) X-ray beam intensity after absorption by the material, and for different directions of irradiations (θ), called projections [26,27]. According to Beer-Lambert's Law, for each angle of projection θ, the resulting intensity $I(y,z,\theta)$ on each pixel of the detector (coordinates y,z) is given by:

$$I(y,z,\theta) = I_0 . \exp(-\int \mu(x,y,z,\theta) dx) \quad (1)$$

where I_0 is the intensity of the beam before the sample and $\mu(x,y,z,\theta)$ the attenuation coefficient along the path of X-ray which hits the pixel of coordinates y,z. The value of the integral of $\mu(x,y,z,\theta)$ for a great number of angles θ is named the Radon transform of the attenuation coefficient of the sample. The projection-slice theorem ensures that, for a sufficient specimen sampling, the 3D map of μ can be reconstructed. The attenuation coefficient mainly depends on the density and the chemical composition of the materials constituting the sample. In the study, aggregates (silica), sound and leached cement paste have distinct μ values. As a result, XCMT is a well-adapted technique to highlight microstructural changes during leaching.

2.2. XCMT used for leaching analysis

High resolution microtomographic acquisitions were performed on the BM05 beam line of the European Synchrotron Radiation Facility (ESRF, Grenoble, France). A monochromatic beam with energy of *35 keV* was used. The acquisition consists in recording *1200* two-dimensional (2D) radiographs at equally spaced angles between *0°* and *180°* (Fig. 1). A scintillator is set behind the sample to convert, as efficiently as possible, X-rays to visible light. Contrast obtained on the 2D projections results from the difference in X-ray absorption by the phases/features encountered by X-rays in the specimen. A mirror and the optical set-up selected for the experiment directed the light to the detector. The FRELON CCD camera, developed at ESRF, comprises *2048 x 2048 pixels*. A pixel size of *5.30 x 5.30 μm^2* is then obtained. The 2D radiographs were, as previously explained, exploited to reconstruct the volume of the samples using the conventional filtered back-projection algorithm [28].

2.3. Material choice, specimens design and accelerated leaching process

The sample size was imposed by the microtomographic analysis. As all the projections must fit the field of view of the camera, the maximal size was of 2048 x *5.30 µm* (about *10 mm*). Cylindrical cores of *8 mm* diameter have been directly obtained from classical prism *40x40x160 mm^3* (Fig. 2). Their lengths varied between *20* to *30 mm*. To perform this study, different cementitious composites have been prepared: the key idea was to reproduce cementitious composites initially proposed by Bisschop and van Mier to study effects of drying on microcracking [29,30]. Here, the focus is put on a composite comprising *35 %* of glass spheres within the cement paste (cement CEM II/B 32,5R with water by cement ratio equal to *0.5*). The glass spheres diameter is *2 mm*. Samples of *8 mm* diameter and *20 mm* long can be considered as representative of the material. Before microtomographic analysis and leaching process, samples were preserved from desiccation in order to avoid any risk of microcracking induced by drying.

In order to analyze different leaching states of the cementitious composite in a reasonable time (at most *6 days* corresponding to the beam time provided by ESRF), an accelerated test able to reproduce long-term material response is required. It was thus chosen, considering the geometry of the specimens, to leach the material by means of an accelerated test with ammonium nitrate solution (NH_4NO_3 – *480 g/kg_{H2O}*). Such leaching process has a very high kinetics (about 300 times the kinetics of leaching by deionised water) and the ammonium nitrate-based calcium leaching leads to the same mineral end products in the cementitious material [16,31].

Despite a crack detection objective, it must be noticed that this microstructure analysis is not able to detect very small microcracks: visibility of microcracks depends on the resolution of the tomographic set-up (here a pixel size of *5.30 µm*), which means that cracks with width larger than *10 µm* can be undoubtedly identified. All cracks having a width smaller than *5 µm* were undetected in the present experiments.

3. Analysis of experimental results and principles of the numerical simulation of microcracking due to leaching

3.1. Experimental procedure and numerical simulation

Numerical simulations were performed on several cross-sections of a sample at different stages of leaching. These cross-sections have been extracted from 3D reconstructed images of a cementitious composite containing 35 % of glass spheres in a cement matrix. They

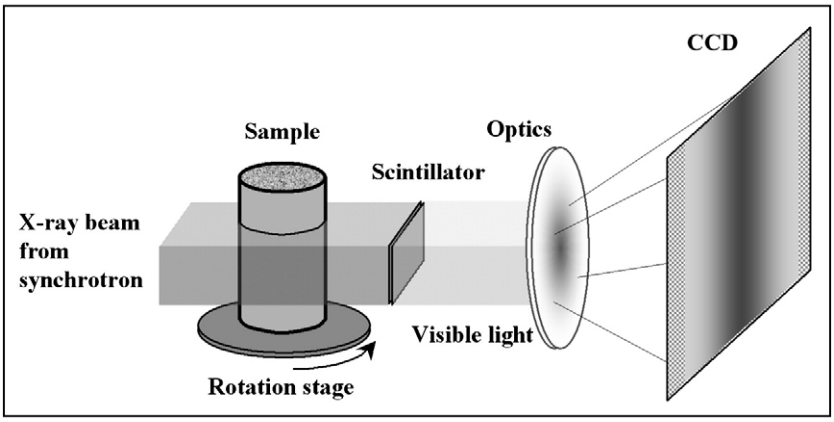

Fig. 1. Sketch of the experimental setup for microtomography mapping.

Fig. 2. Different cementitious composite specimens ($\phi 8$ *mm*) after various degradation processes (leaching, drying and thermal exposure).

have been selected in the middle of the sample, the leaching front is then not perturbed by the upper and lower edge of the sample. A two-dimensional simulation, with plane strains hypothesis, was chosen for the sake of simplicity, even if this assumption will not be able to exactly model the complex 3D geometry and chemico-physical phenomena. The presence of randomly spread glass spheres inside the specimen will restrain axial shrinkage of the cementitious matrix, implying tensile stresses in the axial direction. Moreover, the cracks are *a priori* expected to nucleate around spheres (restraining matrix over rigid inclusions); stresses and strains in these areas should be the best described. The real triaxial state of stresses appears to be better modelled by the plane strains hypothesis (biaxial orthoradial tensile stresses around inclusions) rather than in plane stresses (only uniaxial orthoradial stresses in the plane of the section). Far from any inclusion, the plane strains hypothesis is nevertheless worse, since axial tensile stresses are surestimated (see §5.4).

After the first scanning of the sound sample, it was immerged for 11 hours into the ammonium nitrate solution. This solution was regularly stirred during the total leaching period (96 h for the considered sample). A new acquisition is then made, and the sample is again dipped back into the aggressive solution. New image acquisitions are performed regularly during leaching. The experimental advantage is the possibility to directly compare data obtained with the same sample. A statistical analysis is therefore unuseful. The analysis and the comparison of the various degradation stages are directly made without interference between the leaching process and the experimental device. This allows accurate measurement of the porosity evolution, of the degradation kinetics or of the development of microcracks. The numerical simulation is mainly performed to try to highlight the involved mechanisms. As concerning quantitative data from X-ray microtomographic analysis, and notably exploitation of 3D data, future improvements (image registration, segmentation …) are still needed to obtain for example a reliable quantification of the evolution of cracking. A first step can be achieved by applying a threshold filter to convert gray scale image into binary one, therefore segmenting "voids" (porosity, cracks) from "solid". Crack opening, connectivity for instance can be determined (at the chosen resolution). The recent work of [32] proves that quantitative data of the microstructure from microtomographic acquisition can be obtained, but were not the main goal of this paper.

After numerical 3D reconstruction by back filtered projection, 3D mappings of μ were obtained at the different stages of the sample leaching. On the resulting 3D images, attenuating materials appear in white and non attenuating (porosity or microcracks) in black. Any cross section through the sample can be visualized. Fig. 3.a shows a cross-section of the sound sample in which one can easily identify the glass spheres and the cement matrix. On the left part of the Fig., there are small black discs (i.e. large pores) in which Portlandite crystals had developed. The studied cross-section has been chosen because of the geometrical distribution of the glass spheres (interactions between spheres), and also because of the possible interaction between spheres and the sample surface. As the observed glass diameter distribution is well representative of the sample, this cross-section was chosen for modelling. For simplicity, some glass spheres were not taken into account. Fig. 3.b shows a cross-section in approximatively the same position (same distance from the sample top than Fig. 3.a) after an *11-hour* period of leaching (1st step of leaching), and the Fig. 3.c and 3.d after *18* and *24 hours*. Contrary to Fig. 3.a, the cement matrix is not homogeneous: exterior part of the sample appears darker. It is due to calcium dissolution leading to increase in porosity [14]. A simple analysis of microtomographic data can be performed to quantify the change in gray levels due to leaching inside the specimen. The Fig. 4 shows this evolution along a radial section line from external to internal part of the sample. A strong decrease in gray intensity can be observed when Portlandite is dissolved, then smooth decrease during mainly CSH decalcification, validating the mechanisms of degradation, and computing kinetics of the reaction. This should be useful to better study degradation in pre-cracked samples (as modelled in [33]), but was not dealt with in the present paper. In addition, a small layer of dense material (exterior part of the specimen), supposedly attributed to some carbonation due to the conditioning process, slightly delays the evolution of the leaching front at the beginning of the leaching (this phenomenon is not studied here more precisely). Due to leaching, microcracks appear, particularly near the glass spheres. The leaching front induces a drastic deterioration of cement mechanical strength: as the zones around aggregates are stressed, any decrease in tensile strength may lead to microcracking. Such a microcracking can be detected only with non destructive methods like microtomography. As leaching is mainly linked to the diffusive properties of the cement matrix, the leaching front appears to be a cylinder only slightly influenced by the presence of glass spheres.

A simplified numerical simulation will help to prove such an hypothesis. Each step of leaching is numerically reproduced with the assumption that each leached ring (named *CP1* to *CP4* in §4.1) has its mechanical properties reduced compared to sound material. In Fig. 3.d, one can notice that a network of microcracks occurred and cohesion between the matrix and the glass spheres is very degraded. An example of a 3D-reconstruction is given Fig. 5, where is presented a slab (about *0.25 mm*) of the sample after 18 hours of leaching. Aggregates are in grey, sound cement in light grey and leached cement in dark grey. One clearly distinguishes the 3D crack connecting the surface of the glass sphere to the sample surface. There was no crack, at the spatial resolution of this microtomographic analysis, prior to this experiment.

3.2. How to model the leaching front evolution?

The progression of the leaching front is modelled numerically by considering several layers in the sample volume, each of them

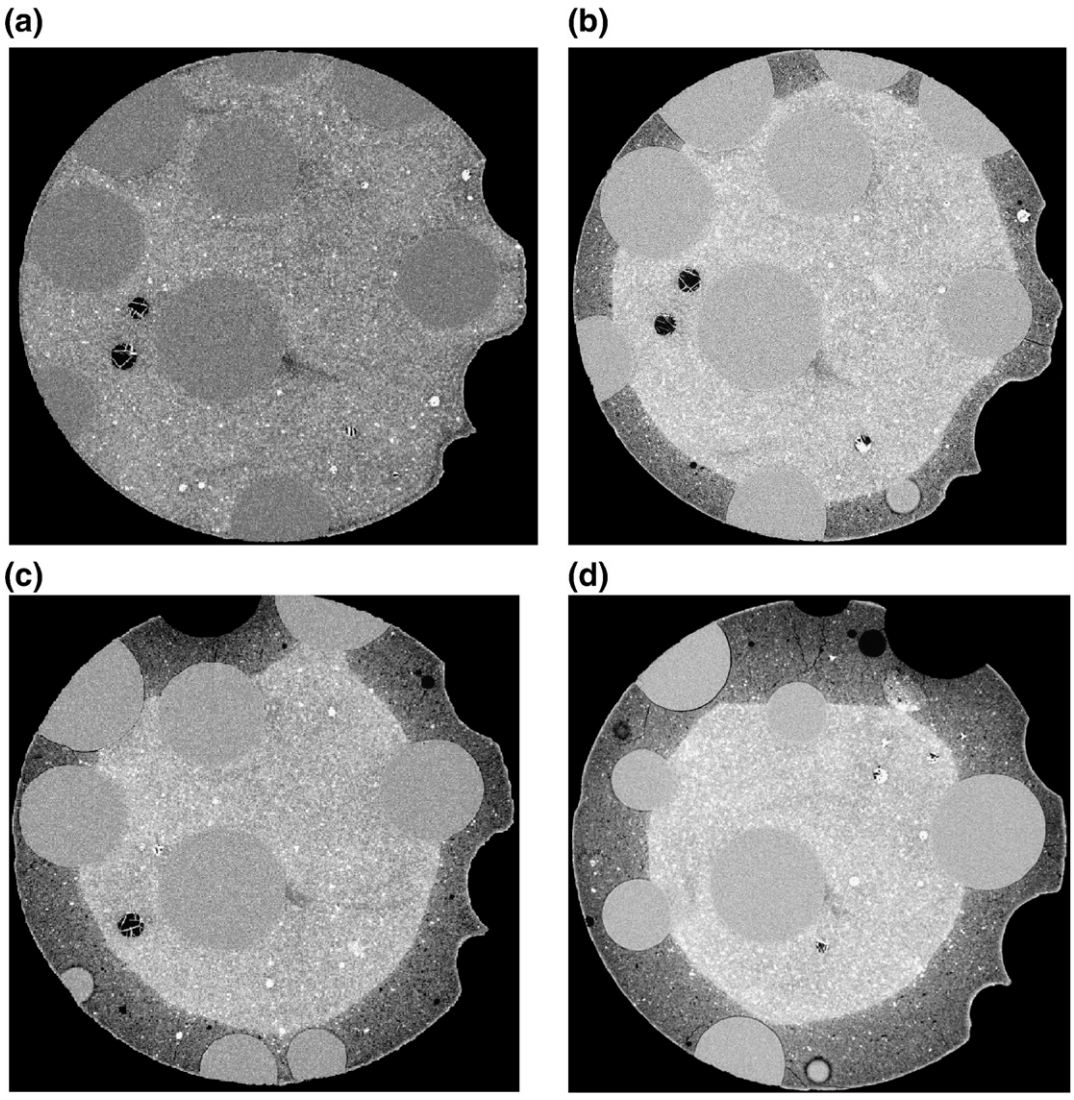

Fig. 3. a. Cross-section of the sample: sound state before leaching. The diameter of the sample is equal to *8 mm*. The glass sphere diameter is *2 mm*. b. Cross-section of the sample after *11 hours* of leaching. c. Cross-section of the sample after *18 hours* of leaching. d. Cross-section of the sample after *24 hours* of leaching.

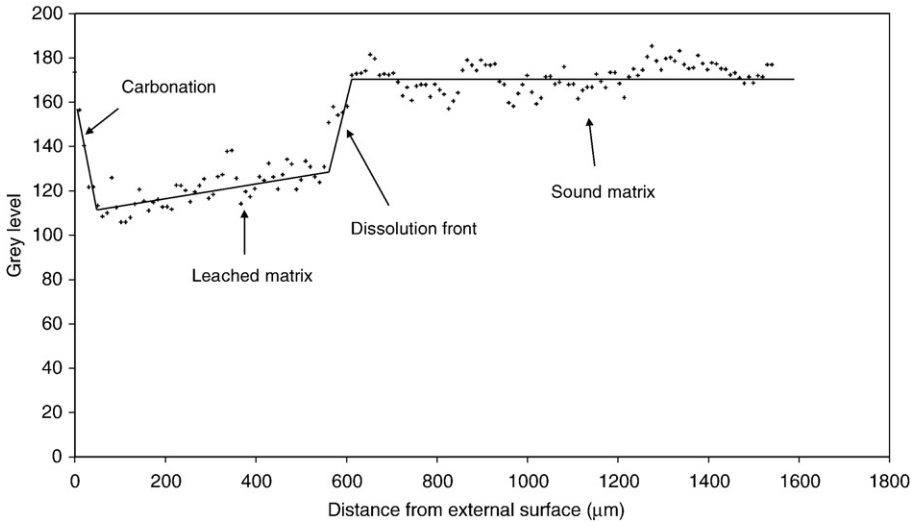

Fig. 4. Evolution in grey levels versus distance from the external surface for a composite leached during 11 hours.

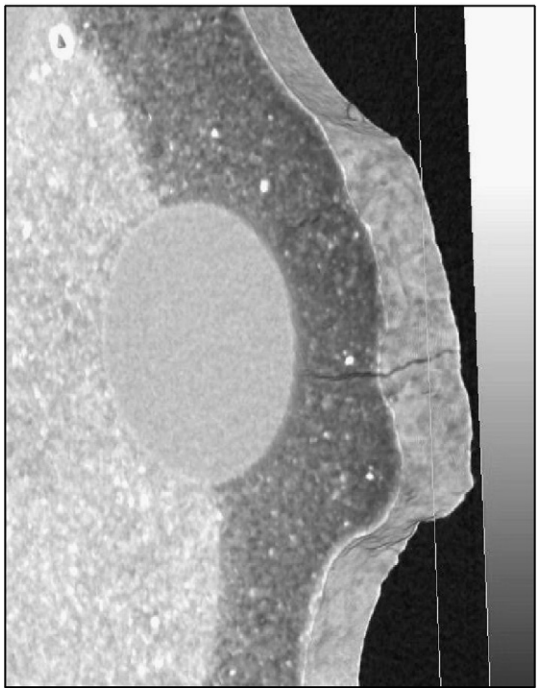

Fig. 5. 3D-reconstruction of a slab of the leached sample during *18 hours* – zoom on the right side of the Fig. 3.c.

corresponding to a step characterized by X-ray microtomography. Taking in consideration effects of leaching process over cement paste, their mechanical properties will decrease gradually. The finite element code used is CESAR LCPC® v4, and more specifically the module CLEO2D which solves two-dimensional problems. The leached state is modelled by a high drop in mechanical properties of cement paste. Such a decrease is commonly observed even at an early leaching [4,6–8]. Fig. 3.b is a slice of the specimen after an 18-hour leaching. The limit between these sound and leached part is highlighted with a large contrast difference. Glass spheres, made of silica, are not degraded and their mechanical properties are not affected with leaching.

The constitutive laws used for glass spheres are isotropic linear elasticity, and elastic-perfectly plastic, simulated with the Mohr-Coulomb criterion, for cementitious matrix, where plastic strains are controlled by stresses. This criterion is widely used for a large variety of materials including concrete [34], and therefore the problem of strain localization does not exist (no softening). The energy stored in the material, previously to leaching (see §3.4), is supposed to be dissipated by plastic strains during leaching, as the plastic domain is supposed modified by the decalcification of the cement matrix. A better description of the role of leaching over mechanical response of the specimen could be performed by using the framework of chemoplasticity [35] for instance. This should lead to a correct definition of the plastic multiplier. The damage could also be taken into account, based on work of Ulm et al. [33]. Moreover, a fully chemo-mechanical coupled model, with a progressive dissolution of calcium, rather than this discrete approach, would be studied in a future work However, the assumptions taken in the present model appear to be at least valid from a qualitative point of view, even if exact crack opening or plastic strains cannot be obtained with this simplified approach.

3.3. Analyzed values

Stress field and the plastic strain norm are calculated after each step of leaching. They are used to exhibit either preferential areas of plasticization or evolution of stresses in the sample. The cracking pattern is potentially known, as models directly based on plastic variables [36] give a link between plasticity and the area where crack will preferentially propagate. Moreover, it should be possible to observe crack closing due to stress relaxation during the progression of the leaching front.. The norm of plastic strains $||\varepsilon_p||$ is defined by Eq. (2).

$$\left\|\overrightarrow{\varepsilon_p}\right\| = \sqrt{\varepsilon_{Ip}{}^2 + \varepsilon_{IIp}{}^2} \tag{2}$$

where ε_{Ip} and ε_{IIp} are main plastic strains.

In the elastic domain, the volume variation around a node of the mesh is expressed by Eq. (3), and shows whether cracks are closing:

$$\frac{\Delta V}{V} = tr(\varepsilon_e) = \frac{3(1-2\nu)(\sigma_I + \sigma_{II} + \sigma_{III})}{E}. \tag{3}$$

with ε_e the elastic strains tensor, σ_I, σ_{II} and σ_{III} the main stresses, $\frac{\Delta V}{V}$ the volume variation, E the Young's modulus and υ the Poisson's ratio.

3.4. Stresses in the samples

Sample is cored in a *40*40*160 mm* prismatic beam cured in lime-saturated water for *28 days*, and then protected of desiccation for *6 months* by a self-adhesive aluminium film. During this time, the beam was initially submitted to the Le Châtelier contraction and then to endogenous shrinkage. The prismatic beam being hydraulically isolated from its environment, shrinkage depends on capillary pressure decrease due to saturation decrease caused by water consumption during cement hydration. Shrinkage was regularly monitored with a linear transducer measuring a linear variation of length with time. As the composite is supposed isotropic, the volumetric shrinkage is equal to three times the one dimensional shrinkage. To model the effect of endogenous shrinkage on the sample cored from the prismatic beam, cement paste is initially submitted to thermal strain $\varepsilon_{thermal}$ equivalent to endogenous shrinkage strain $\varepsilon_{endogenous}$.

Decalcification is another cause of autogenous stresses during leaching [16]. In each new leached layer, decalcification increases stresses in the material by increasing strains, and tends to increase plastic strains. A parallel study has been conducted taking into consideration this effect by applying, before the leaching of a new layer, decalcification shrinkage in this layer (by means of the same thermal analogy).

4. Numerical model: from X-ray microtomography to finite elements calculations

The numerical sample, issued from X-ray analysis and presented in Fig. 6, comprises 7 glass spheres (#1 to #7) located as they are in the reference slice before leaching (Fig. 3.a). To concentrate analysis on representative cases, only these 7 aggregates have been selected, since they depict almost all geometrical dispositions (Fig. 6). For instance, an aggregate far from the surface of the specimen, (#7), or on the contrary close to the surface (#4 and #6), an aggregate partially out of the sample (#1, 3 and 5), neighbour aggregates (#1, 6, 2 and 3), and finally under an asperity of the surface (#2). This geometry seems adequate to explain crack openings and besides, to extrapolate these results to other distributions.

These glass spheres are inclusions into a cementitious matrix, which has been divided in 4 layers (approximately 1 mm-thickness for *CP1* and *CP2* layers, *2 mm* for *CP3* and *CP4* is the central part of the specimen). Their mechanical properties will strongly decrease when the front of lixiviation will progress into the material.

The generated mesh is composed of about 3 850 6-nodes triangles (quadratic interpolation). At each interface between aggregates and cement paste, 6-nodes interface elements are added (151 elements),

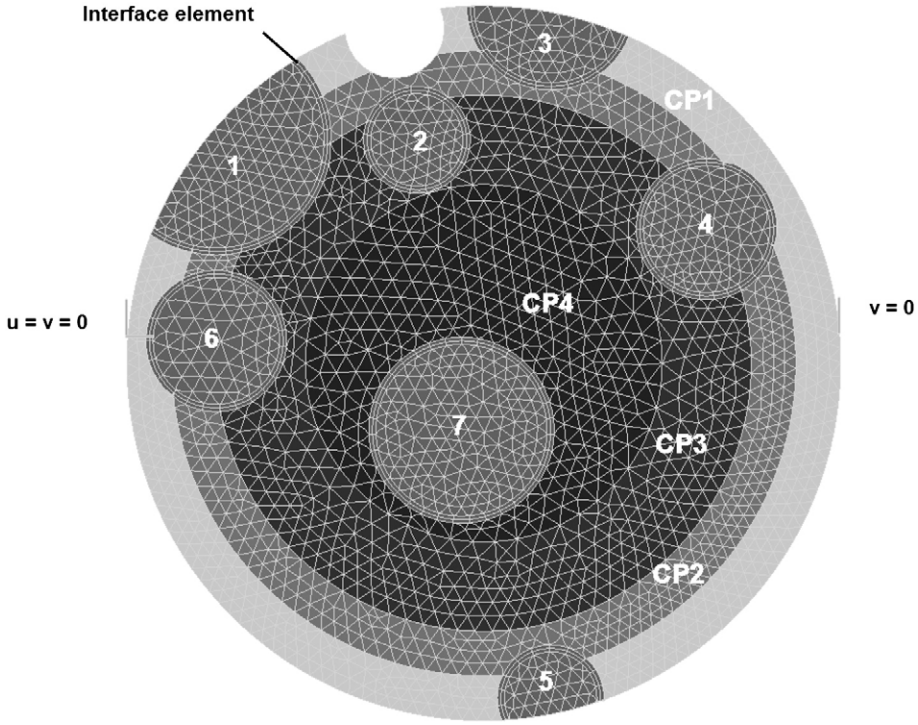

Fig. 6. Mesh used in the model (*u* and *v* are respectively horizontal and vertical displacements, aggregates are numbered from *1* to *7* and cement layers from *CP1* to *CP4*).

allowing to model the interface behaviour with, as for cement paste layers, two different states: sound or leached. The parameters and properties were not deduced to fit experimental and numerical results. Rather than using a complex model with lots of parameters which cannot be easily measured experimentally, and where a parametric study should be essential, the purpose was clearly different. The objective was to set up a numerical approach where the maximum of properties are known, to attempt to validate the mechanisms leading to cracks, and not to be able to precisely describe the cracking pattern (density of crack, crack opening…). Values of the parameters required by this model are summarized in Table 1: glass spheres [37], sound and leached cement paste [2,7]. The internal friction angle φ has been estimated from the friction coefficient δ. C is the cohesion of the material and E its Young's modulus. The Poisson's ratio ν of the sound cement paste is *0.24*, in accordance with values generally reported in the literature, between *0.2* and *0.25* [38,39]. Because of lack of experimental data, Poisson's ratio is assumed to be constant despite leaching.

Interface elements allow modeling the matrix-aggregate interface (also named Interfacial Transition Zone) which is, mechanically speaking, very weak compared to cement paste or glass. Indeed, aggregate surface is smooth and rounded, avoiding creation of a tough link between the constituents. This was noticed by several authors [29,30]. Moreover, glass is non-porous therefore reinforcing this interface weakness. Strong colloidal bridges are almost impossible. This was taken into consideration, assuming Coulomb's friction at this interface, with a low value for the friction threshold. As previously explained, two situations were considered: the so-called sound interfaces around aggregates for which less than half of the perimeter has been attacked, and the degraded interfaces in the other cases. The modelling parameters and properties are extrapolated from cement paste data from the literature. Young's modulus of interface is approximately 50% lower than matrix's one [40–42]. Tensile strength (*Rt*) is supposed low: initially 1.5 MPa, and 1 MPa after leaching. These values are in accordance with tensile strength measured for cement paste [43], which was 1.87 MPa before leaching and 0.87 MPa after. To model the interface weakness, arbitrary low values of the two Coulomb friction parameters (*C* and φ) were chosen (see Table 2). We can notice that for a "real" aggregate (not a sphere), the values would have been different, modelling the influence of an higher roughness. Friction, separation and non-interpenetrability conditions are taken into account.

The simulations are done with the following stop criterions: maximum of 1000 iterations and a tolerance of 0.1% for convergence of the solution. The plane deformation hypothesis induces stresses in the axial direction of the specimen (Z-axis) as explained in §3.1.

The initial homogenous strain due to maturation measured is *-300 micro-strains*. By thermal analogy (*cf.* §3.4), equivalent thermal stresses induced by endogenous shrinkage are modelled by a temperature variation of *-30 °C* of the cement paste (dilation coefficient $\alpha = 10^{-5}$).

About the shrinkage due to decalcification, the radial displacement is taken from the work of Chen et al. [16] and varies with calcium to silicium (Ca/Si) ratio of solid. Since the simulations only consider 2 states (sound or leached) for cement paste, *5500 micro-strains* are assumed to be representative of the completely leached state of the cement matrix. However, this radial shrinkage is measured on leached specimen, whereas in the model this shrinkage is applied on cement paste just before leaching, which means on sound state matrix. To be

Table 1
Mechanical parameters used for each constituent.

	E (MPa)	ν	C (MPa)	φ (°)
Sound cement paste	22800	0.24	17.1	54.9
Leached cement paste	3600	0.24	1.3	34.1
Glass aggregates	73000	0.17	-	-

Table 2
Properties of interface elements.

	E (MPa)	Rt (MPa)	C (MPa)	φ(°)
Sound interface	11400	1,5	2	35
Leached interface	1800	1	1	25

equivalent in stresses, since the Young's modulus of the cementitious matrix is divided by about *6* with leaching, the microstrains to take into consideration is one-sixth of *5500*, so about *900 micro-strains*.

5. Analysis of numerical results

5.1. Locations of studied lines

To clearly analyse results of the simulations, several lines are examined (Fig. 7), where evolutions in cement paste and glass spheres are observable. Selected lines (named AA' to FF' and GM to JM) give a more precise view of the evolution of stresses and strains during leaching. All the profiles along these lines are not presented here, except profiles along JM, since sections with isovalues are sufficient for explanations, and location of selected lines allows highlighting where the reader has to focus.

The orientation of the lines is given by arrows on Fig. 7. The line origins are the first point of the line (H is the origin for line HM), and the last point is the end of the line. On profiles presented in next paragraphs, the term "position on the line" stands for the axis-coordinate in the local reference mark so defined and oriented.

5.2. Leaching without decalcification shrinkage

Prior to leaching, the mature sample is modeled only by taking into account the thermal strain equivalent to maturation endogenous strain. Even in this state, numerical simulation shows that the sample is submitted to severe stresses, mainly around aggregates, as seen in Fig. 8 representing plane main stresses at each node of the mesh. A large part of the cementitious matrix is in tensile state, since rounded aggregates restrain free shrinkage during maturation. Respectively, aggregates are only in compressive state, because of endogenous shrinkage which acts as a pressure around them. Physically, the difference in Young's modulus between cement paste and glass explains this phenomenon [44]. Indeed, shrinkage is higher in cement paste than in aggregates. However, no plasticized area appears in the matrix. This evidence confirms visual observations made in Fig. 3.a, where no crack was detected at the mesoscale (*1 pixel = 5.30 μm*).

At the following stage (11 hours of leaching), the first external layer (*CP1*, thickness = *1 mm*) is considered as totally leached and its mechanical properties are uniformly degraded. Results presented in the following show the location of zones of important plastic strains (Fig. 9, a darker colour means a higher plastic strain norm). They are located close to aggregates in periphery of the sample. Indeed, as underlined in the previous paragraph, areas heavily submitted to tension are around aggregates, where free strain is inhibited. Moreover, strength of cement paste decreases with leaching. So, plasticization (or microcracks) is likely to appear in these areas. Aggregates at subsurface of the sample (#4 and #6) lead to highest plastic strains during leaching of the first external layer. This is because, in this zone, thickness of cement paste is very low.

After *18 hour* of leaching in ammonium nitrate solution, *CP2* layer is now considered as totally leached. That corresponds to the state

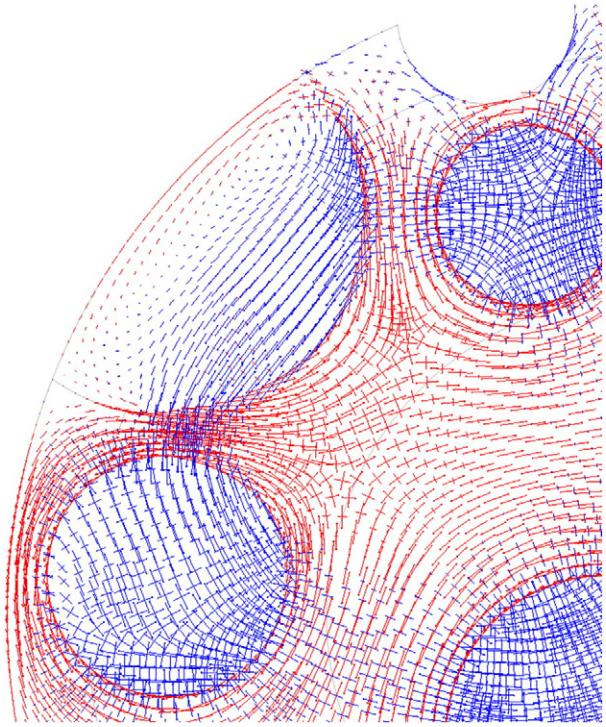

Fig. 8. Representation of the main stresses' tensor in each node of the mesh (in red, tensile stress and in blue compressive stress, length of segments is proportional to intensity of stress. Axial stresses are not represented.

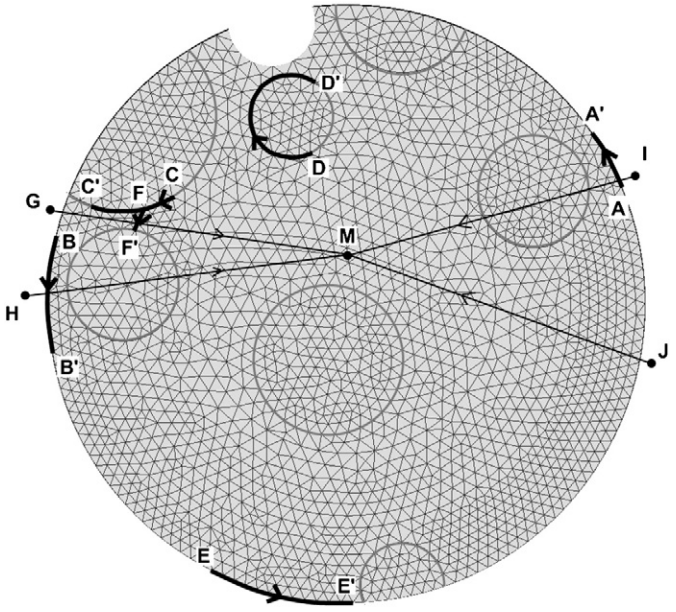

Fig. 7. Localization of selected lines (lines AA' to FF' and GM to JM). Arrows indicate the orientation of each line.

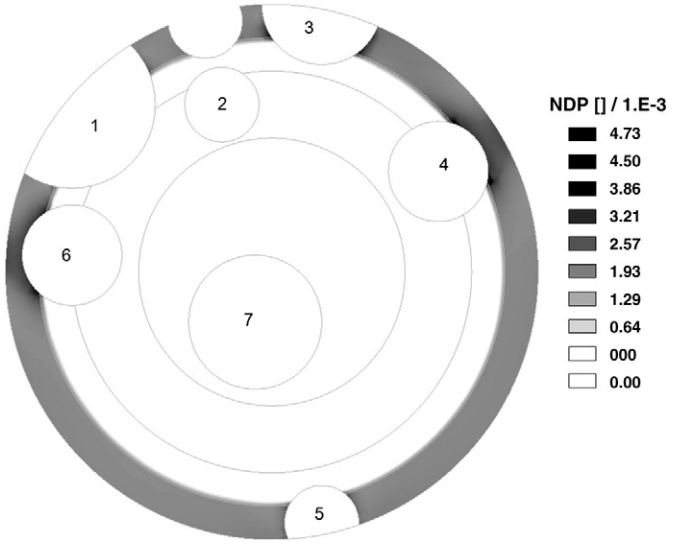

Fig. 9. Isovalues of the norm of plastic strains (NDP) after leaching of the layer *CP1*. Scale is given at the right of the schema (from *0* to *4.73 10^{-3}* strains).

observed in Fig. 3.c. Fig. 10 presents the map of plasticized zones close to aggregates #1, #6 and #2. Concerning cracks opening, there is a very good qualitative concordance between numerical simulation and experimental observations on Fig. 3.c. The remark made in the previous paragraph about repartition of plasticized zones around the aggregates is confirmed with the leaching of *CP2* layer.

Zooming onto aggregate #6 (Fig. 11) allows to make a comparison between numerical simulation (Fig. 10) and reality observed by means of X-ray microtomography. Therefore, a strong agreement exists between zones where plastic strains are important and the localization of cracks. In particular, the crack (b) of Fig. 11 perfectly matches with numerical model (Fig. 10). In addition, studying more precisely aggregates #1 and #6, the maximum plastic strain deformation norm is located on the shorter way between their surfaces (crack (a) in Fig. 11). Both aggregates prevent free shrinkage of the cement paste, and their proximity creates an overlapping of the associated plastic areas. This overlapping leads to a dramatic increase of the plastic strain norms. For more distant aggregates (#1 and #2, or #2 and #3, for instance), plasticization becomes lower.

Another remark can be drawn on apparition of plasticity close to aggregate #4 (the line IM, Fig. 7, passes through the area of higher plastic strain around aggregate #4). Propagation of plasticity globally occurs from the surface of the aggregate towards the periphery of the sample, and not the inverse. This could be explained since stresses become higher when approaching the aggregate surface. However, studying aggregate #6 and the profile along HM (HM passes through the diameter of the glass sphere but not through the maximum of plastic strain around it), it appears that the most important plastic strain is close to the external surface of the sample, and not around the aggregate. In the profile along JM, in plain cement paste (aggregates are supposed not influencing analysed stresses or strains), the maximum of plastic strains is at the external surface of the sample. Two distinct effects would lead to cracking, one coming from the aggregate, and the other one from the cementitious matrix itself. The first one is manifest around each aggregate where cracks exist. Indeed, cracks are larger close to the aggregate and then become smaller. Crack (a) in Fig. 11 illustrates this phenomenon. The second effect can be seen in Fig. 12, which is a zoom over the cement matrix after 24 hours of leaching and far from any rigid inclusion. Cracks initiating from the surface of the sample, and propagating within the sample can be distinguished. No rigid inclusion can explain their apparition. The cause seems to be the difference in Young's modulus between sound and leached layers. This is a structural effect. Cracking (or plastic strains) is a sum of these two physical effects. Close to an aggregate, the first effect will be predominant, whereas it is the second one in parts where effects of inclusions are negligible. This structural effect in cement paste is more precisely studied in §5.4 which deals with leaching of samples where glass aggregates are replaced by polystyrene spheres.

Finally, plasticization in cementitious matrix when aggregates' effects are negligible is almost uniform in the model, whereas in reality, cracks in cement paste are local. Nucleation of cracks is

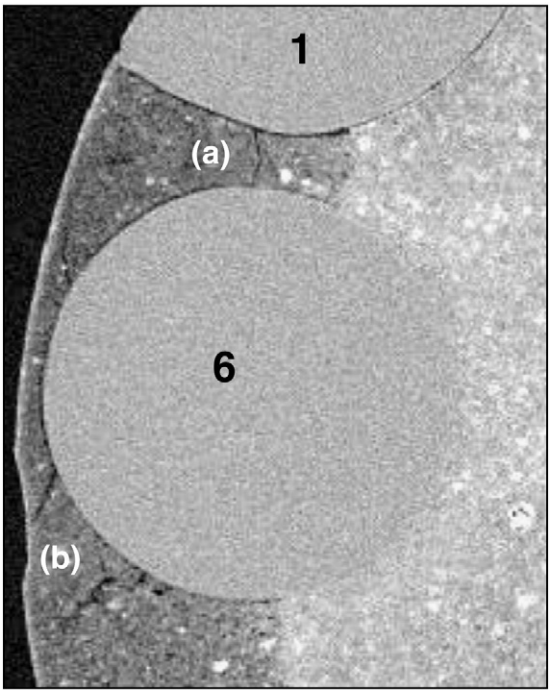

Fig. 11. Zoom on aggregate #6 after 18 hours of leaching: (a) cracking between two neighbour aggregates, (b) cracking between subsurface aggregate and surface of the specimen.

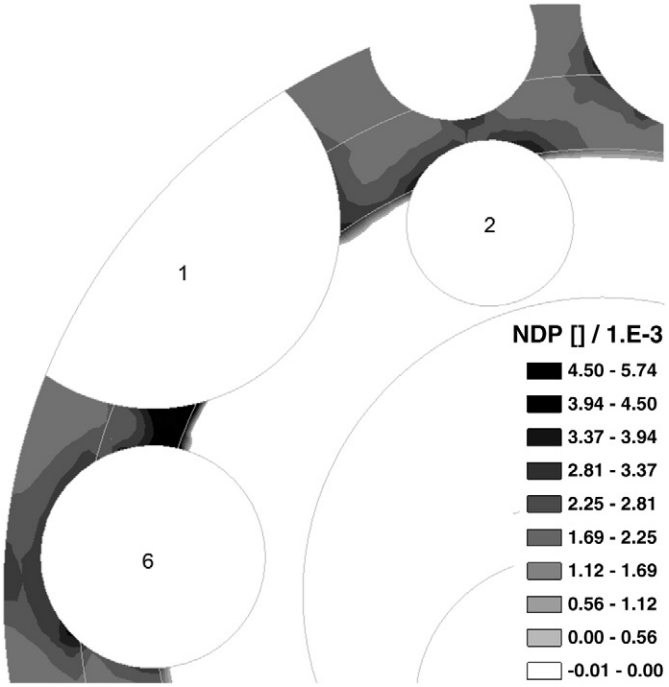

Fig. 10. Isovalues of the norm of plastic strains close to aggregates #1, #2 and #6 after leaching of *CP2* layer. Each level of grey corresponds to an interval of values.

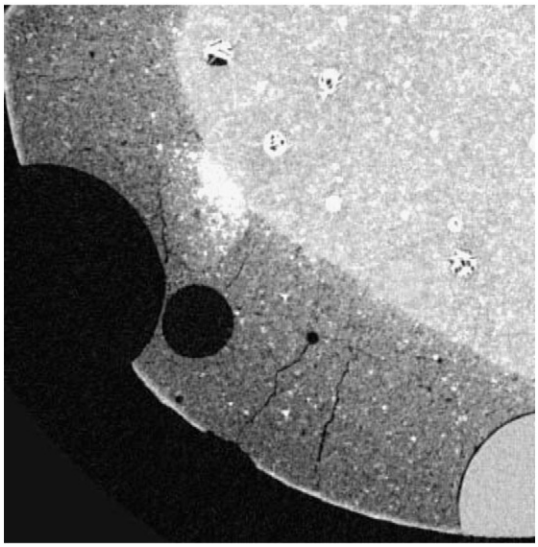

Fig. 12. Zoom on matrix far from any inclusion after a *24-hour* leaching – the asperity was present before leaching.

probably due to a local defect. This effect was not taken into consideration in the model, for which cement paste is considered homogeneous as seen in Fig. 3.a (anhydrous cement, porosity…). Then, degradation due to leaching continues on the other layers (*CP3* then *CP4*), on the same way that previously. Plasticized areas in periphery of the sample, which had appeared after leaching of *CP1* and *CP2*, do not evolve when *CP3* and *CP4* are leached. Plasticization only progresses in new leached layers.

An interesting phenomenon has to be highlighted. Examining the evolution of the norm of plastic strains with respect to evolution of main strains the section JM, the latter tend to decrease whereas the front of leaching is progressing (Fig. 13). When *CP1* is leached, there is a severe decrease in main stresses in *CP1* layer. This fact is due to a diminution of its mechanical properties, which goes hand in hand with an increase in the norm of plastic strains (Fig. 13.a). In the next step, during leaching of *CP2*, the same phenomenon is observed in this layer. However, studying the behaviour of *CP1*, plastic strains do not evolve anymore. In addition, the sum of main strains, which are elastic strains if the yield function is negative, tends to slightly decrease. So, when *CP2* is leached, there are relaxations of stresses inside layer *CP1*. A possible crack in *CP1* would have a tendency to partially close when next layers are leached, as total strains are decreasing. This assumption is verified when *CP3*, then *CP4*, are leached (Fig. 13.b). Arrows indicate the diminution of volume strains (whereas the norm of plastic strains does not evolve as it is shown in Fig. 13.a) with progression of the front of leaching. An analysis of the other sections shows similar behaviour (even if it can be less pronounced). Numerically, it is possible with a relatively simple model to confirm experimental observations, and to simulate that cracks open then close partially with the progression of the front of leaching.

5.3. How does the decalcification shrinkage influence the behaviour of the specimen?

A parallel study has been conducted to show how decalcification shrinkage could modify the behaviour of the specimen submitted to leaching. A comparison was made between isovalues of plastic strains norm with (Fig. 14.a) or without (Fig. 14.b) taking into consideration

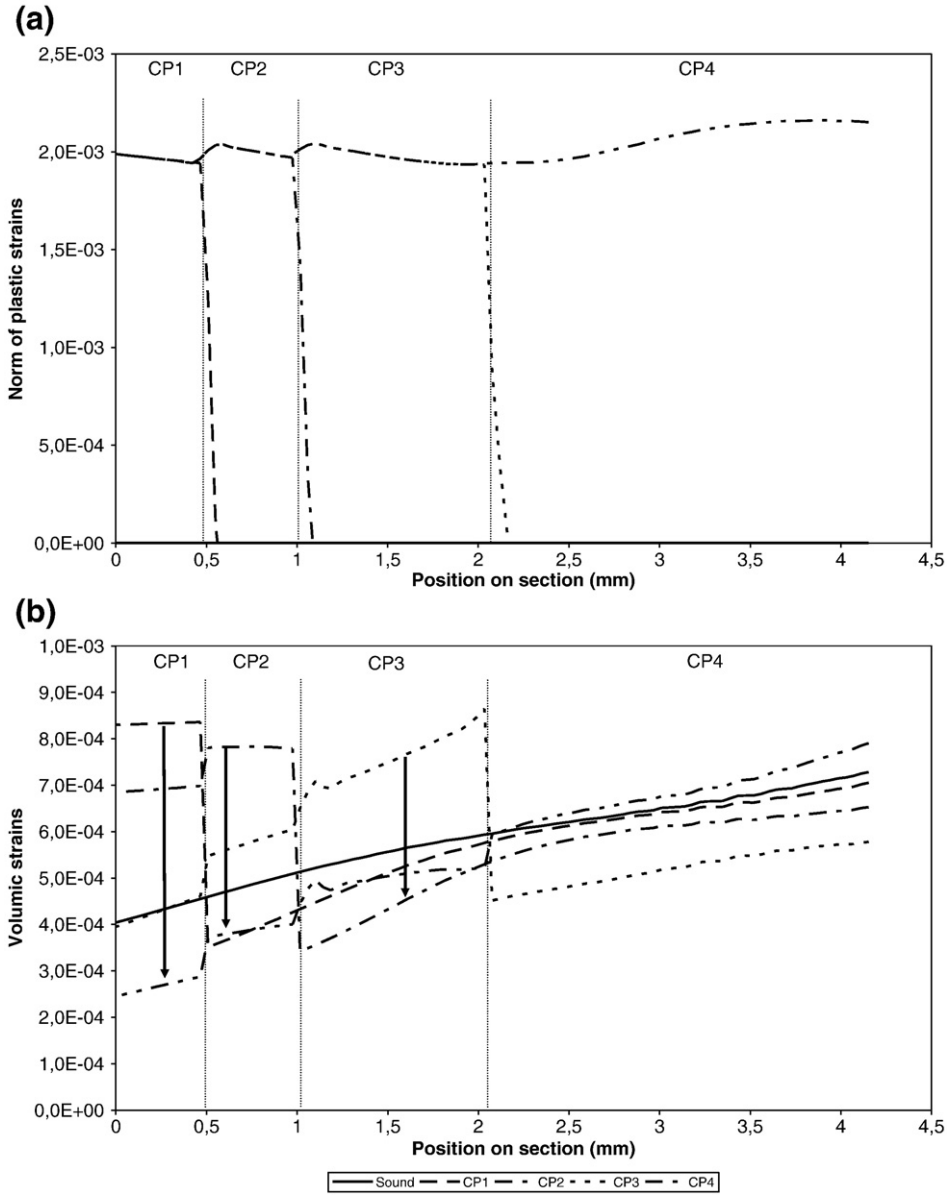

Fig. 13. a & b. Evolution during leaching (sound sample in ——, *CP1*-leached in – – –, *CP2*-leached in – – – , *CP3*-leached - - - et totally leached in – - - –) of the norm of plastic strains (a) and of volume strains (b) on JM section. Arrows on (b) indicate a decrease in elastic strains during leaching (when plastic strains do not evolve).

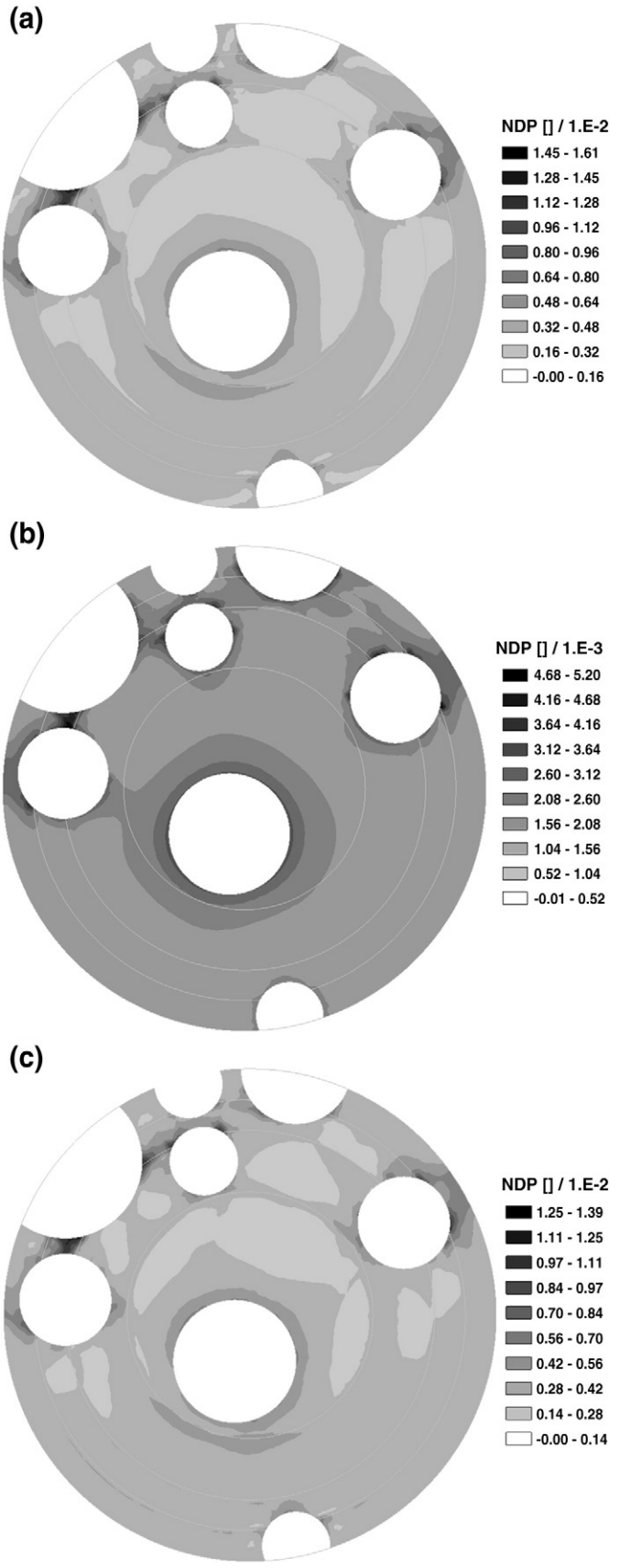

Fig. 14. a. Isovalues of the norm of plastic strains, induced by both endogenous and decalcification shrinkage, for the sample totally leached. b. Isovalues of the norm of plastic strains, induced only by endogenous shrinkage, for the sample totally leached. c. Isovalues of the norm of plastic strains, induced only by decalcification shrinkage, for the sample totally leached.

decalcification shrinkage. Moreover, the response of the specimen under only decalcification shrinkage (initial endogenous shrinkage is suppressed) was calculated. Result is shown on Fig. 14.c.

Some partial conclusions can be made: firstly, decalcification shrinkage increases the plastic strains observed in endogenous pre-stressed simulation. It does not completely modify the repartition of the high plasticity areas. It mainly emphases effects of the initial endogenous shrinkage. Moreover, if the endogenous effect is suppressed, similar results are observed. The comparison with experimental cracking pattern demonstrates that decalcification shrinkage or pre-stressing seems to lead to the same qualitative results. If plasticity only occurs in the leached layer (that seems to globally be the case), the sound matrix remains elastic. Adding (or not) shrinkage in the next leached layer will change only the level of elastic stresses. Hence, studying the decalcification and/or endogenous shrinkage can be done by taking into consideration initial pre-stressing only. However, decalcification shrinkage seems to be predominant versus endogenous one as strain levels are three times higher. The cause of cracking appears to be well explained by a state of stresses induced by matrix shrinkage.

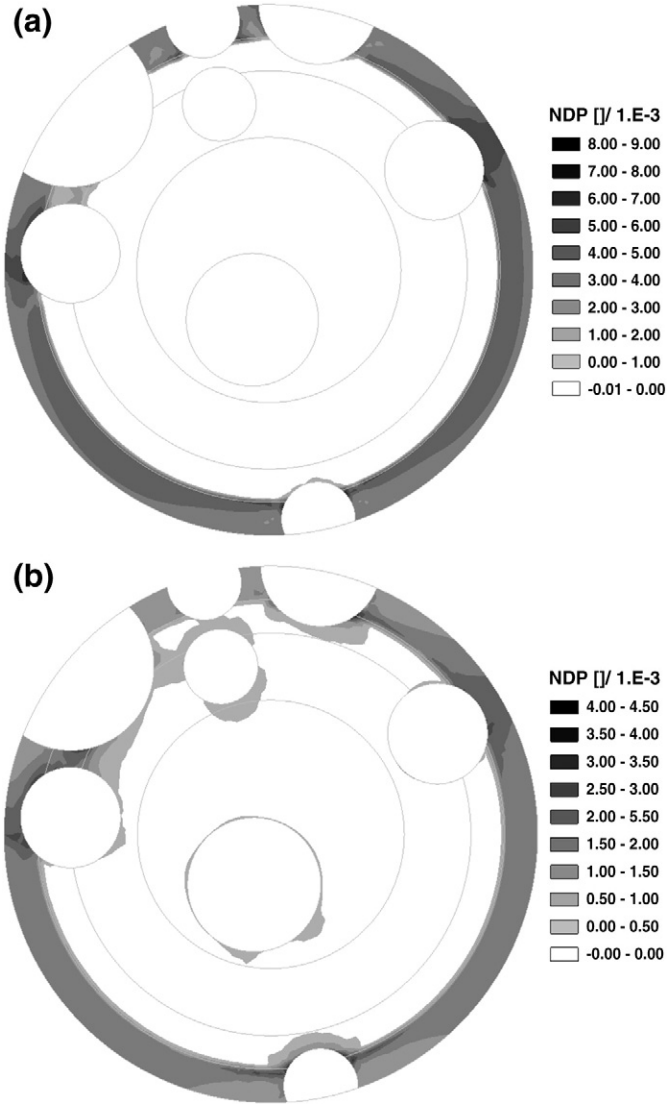

Fig. 15. a. Calculated plastic strains norm of the composite after 11 hours of leaching, with a different interface cohesion (Matrix : $C=17{,}11$ MPa - $\varphi=54.9°$ / Interface : $C=7$ MPa instead of $C=2$ MPa). b. Calculated plastic strains norm of the composite after 11 hours of leaching, with a different matrix cohesion (Matrix : $C=5.04$ MPa - $\varphi=69°$ instead of $C=17.11$ MPa – $\varphi=54.9°$ / Interface : $C=2$ MPa).

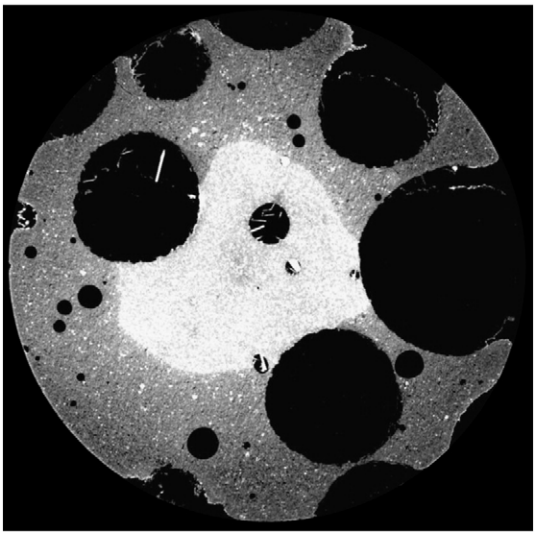

Fig. 16. Cross-section of the polystyrene – cement composite: leached state after *24 hours*. The diameter of the sample is equal to *8 mm*. The polystyrene sphere diameter is *2 mm*.

Finally, some parametric simulations have been performed to study, for instance, the effect of the value of cohesion (of the matrix or of the interface) over plastic strains repartition. The Fig. 15a shows the plastic strain norm, after leaching of CP1, by changing cohesion of the sound interface from 2 MPa (chosen value in the model) to 7 MPa. The Fig. 15b shows the plastic strain norm, after leaching of the layer CP1, by modifying the sound cohesion of the matrix from 17.11 MPa (and friction angle 54.9°) to 5.04 MPa (and friction angle 69°), as proposed in [45] for cement pastes.

Qualitatively, the areas where plastic strains are the highest remain identical, tending to show that the results are not only a consequence of the values, but of the physics of the model (residual strength of the leached material inferior to stresses due to decalcification and endogenous shrinkage).

5.4. Analysis of a cementitious composite with polystyrene spheres

In order to complete and have a better comprehension of the structural effect, a composite where glass aggregates are replaced by voids is studied. This configuration is experimentally achieved by using a cementitious composite made of the previous cement paste with polystyrene inclusions (diameter: 2 mm, volume fraction: 35%). Strains in cement paste are not influenced by rigid inclusions, since the low stiffness of polystyrene, and local effect is therefore eliminated. Only a structural effect could avoid free strains in cement paste, due to a difference between Young's modulus of sound and leached cement paste. X-ray microtomography analysis was done on such a material. The Fig. 16 shows a cross section of the polystyrene – cement composite after 24 hours of leaching. As the density of polystyrene is very low (about *20 kg/m*^{3}) compared to cement matrix, polystyrene spheres are almost transparent to X-ray (darker areas in Fig. 16). No clear microcracking pattern was detected around polystyrene sphere as previously observed in glass-cement composites. However some cracks are visible, but mainly seems to be radial, and probably due to differential shrinkage between sound and leach areas. The polystyrene sphere voids would act as defects where structural radial cracks can nucleate. As a conclusion, from an experimental point of view, some evidences of the structural effect have been highlighted. To confirm this structural effect, the same numerical model, previously described, is used: all glass spheres are replaced by voids to eliminate the local effect. Interface elements are suppressed. Nevertheless, there is an issue in this model due to plane strains hypothesis. In fact, axial strains imposed to *0* generate axial tensile stresses in cement paste. For composite with glass aggregates, this approximation can be made: glass spheres are randomly spread into the specimen, and as stated in §3.1, the triaxial stresses around inclusions were better modelled with plane strains hypothesis. Moreover, axial tensile stresses in matrix may be assumed to be due to existing inclusions in the 3D specimen, which limit the free axial shrinkage of the cementitious matrix. These axial tensile stresses are almost uniform in the model with glass aggregates and do not strongly influence the map of cracks (only the level of the norm of plastic strains is offset, which is not problematic in a qualitative model). For the model where glass spheres are replaced by voids, this hypothesis strongly differs from experimental conditions. Yet, plane strains hypothesis is again done. The first reason is that it is more reliable to compare with exactly the same general hypothesis than the model used for glass-cement composite. The second one, and more important, is that axial stresses are totally uniform. So they only offset values of plasticization uniformly in the specimen, and not locally. There is probably no plasticization in a real sample, but this study could be useful to understand structural effects.

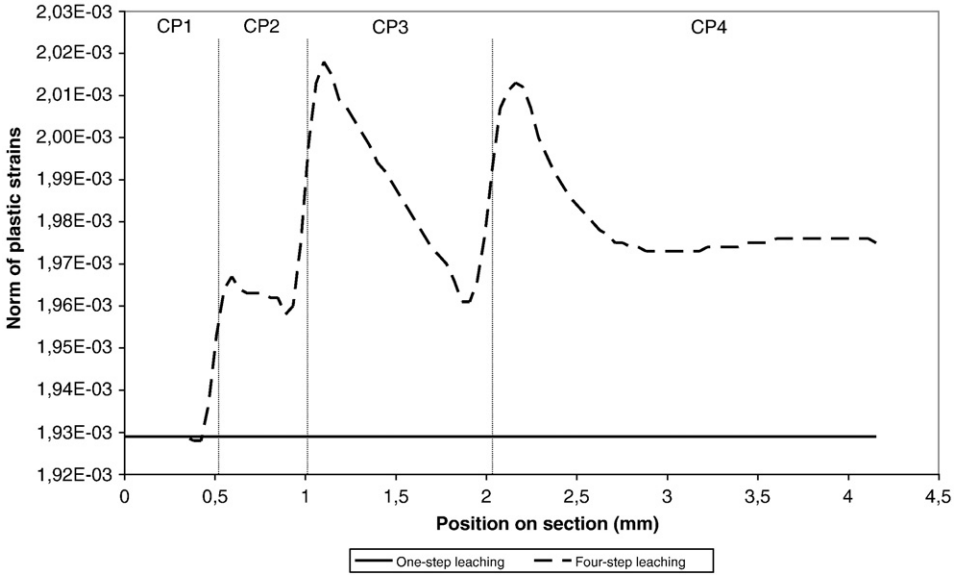

Fig. 17. Norm of plastic strains after four-step (in – – –) or one-step (in ——) leaching (JM section in a totally leached state).

In the model, the cementitious matrix is leached in a progressive leaching as described before (four-step leaching), or in a one-step leaching (the four layers become suddenly degraded). This one-step leaching is considered to suppress the structural effect, since no difference in Young's modulus between sound and leached matrix can exist anymore. The results are shown in Fig. 17, where plasticization is observed on section JM in the two previous cases (one-step leaching in ——, and four-step leaching in - - - -). Clearly, the four-step leaching leads to a higher plasticization and plastic strains are higher on the external part of each layer. This remark tends to confirm that, if inclusions are too far to be influent on matrix behaviour, a structural effect causes cracks, initiated on the external surface of the specimen and which propagate toward the sample.

6. Conclusions

This study was a new experimental approach to identify the existence of a microcracking due to leaching of cementitious composites. The technique used was based on the X-ray microtomographic analysis of a sample progressively leached. The resolution used here was *5.30 micr*ometers. Advantages of such a method led to investigations done on the same sample after several states of leaching. It was then possible to follow evolution of cement microstructure along degradation process. Results on porosity, leaching front or microcracking were obtained on the same sample, without perturbations on cement matrix due to the technique of measurement. Among results, an important one was that leaching leads to microcracking of the cement paste, particularly around rigid aggregates. This microcracking is little opened and partially closes after the passage of the leaching front. An explanation is that cementitious materials are auto-stressed materials due to the endogenous and decalcification shrinkages. Around aggregates, tensile stresses develop, and after leaching and decrease in mechanical properties of cement, induce microcracking.

To confirm this hypothesis, a numerical simulation was performed. This showed that based on Mohr-Coulomb elastoplastic model, it was possible to validate experimental observations on leached cement paste with glass spheres. Occurrences of high plastic strains areas are highly influenced by the rounded glass aggregates, which prevent free strains of the matrix, due to either endogenous or decalcification shrinkage. This phenomenon of a shrinking matrix over rigid inclusion leading to cracks was yet studied for similar cementitious composites submitted to drying [29]. It is there reinforced by a degradation of the mechanical properties of the leached matrix. High plastic strains due to these rigid inclusions begin close to the aggregate surface, and then propagate inside cement paste. This effect is local. If two aggregates are close to each other, the matrix area between them is highly stressed. Cementitious matrix is almost plasticized uniformly if rigid inclusions are so far away that they cannot have an impact on mechanical response to leaching. However, norm of plastic strains tends to be higher at the surface of the specimen than deeper inside. As a result, cracks would nucleate, close to specimen's surface. This phenomenon is more a structural effect, since sound layers are more rigid than leached one, and does not exist anymore when all layers are leached in one time. Occurrence of cracks is mainly caused by these two effects: a structural and a local phenomenon. Damage modelling of leaching processes will be well adapted to numerical simulation of durability problems of concrete structures. Finally, chosen interface elements seem to be adequate to this model.

However, a more complex model could be used in the future, with a damage variable directly linked to plastic strains (see for example [46]). The relevance of using a damage model to predict the mechanical effects of leaching is here consolidated, according to the X-ray microtomographic results. In addition, a transitory regime could be studied, taking into consideration both diffusivity problems linked to leaching process and mechanical.

Acknowledgements

We acknowledge the *European Synchrotron Radiation Facility (ESRF)* for provision of synchrotron radiation facilities, in particular the BM05 team for the technical support during the experiments. We acknowledge also the *French Ministry of Research and Technology* and the *National Research Agency (ANR)* for the partial financial support of our research team by an *ANR Blanche* entitled *MICROFISS*.

References

[1] D. Bentz, E. Garboczi, Modelling the leaching of calcium hydroxide from cement paste: effects on pore space percolation and diffusivity, Mater. Struct. 25 (1992) 523–533.
[2] C. Carde, R. Francois, Modeling the loss of strength and porosity increase due to leaching of cement paste, Cem. Concr. Res. 21 (1999) 181–188.
[3] K. Hagaa, M. Shibataa, M. Hironagab, S. Tanakac, S. Nagasaki, Change in pore structure and composition of hardened cement paste during the process of dissolution, Cem. Concr. Res. 35 (2005) 943–950.
[4] C. Carde, R. François, J.M. Torrenti, Leaching of both calcium hydroxide and C-S-H from cement paste: modelling the mechanical, Cem. Concr. Res. 26 (1996) 1257–1268.
[5] U. Schneider, S.-W. Chen, The chemomechanical effect and the mechanochemical effect on high-performance concrete subjected to stress corrosion, Cem. Concr. Res. 28 (1998) 509–522.
[6] C. Le Bellégo, B. Gérard, G. Pijaudier-Cabot, Chemo-mechanical effects in mortar beams subjected to water hydrolysis, ASCE J. Eng. Mech. 126 (2000) 266–272.
[7] F.H. Heukamp, F.J. Ulm, J.T. Germaine, Poroplastic properties of calcium-leached cement-based materials, Cem. Concr. Res. 33 (2003) 1155–1173.
[8] F. Agostini, Z. Lafhaj, F. Skoczylas, H. Loodsveldt, Experimental study of accelerated leaching on hollow cylinders of mortar, Cem. Concr. Res. 37 (2007) 71–78.
[9] V.H. Nguyen, H. Colina, J.M. Torrenti, C. Boulay, B. Nedjar, Chemo-mechanical coupling behaviour of leached concrete. Part I: Experimental results, Nucl. Eng. Des. 237 (2007) 2083–2089.
[10] B. Gérard, G. Pijaudier-Cabot, C. Laborderie, Coupled diffusion-damage modelling and the implications on failure due to strain localisation, Int. J. Solids Struct. 35 (1998) 4107–4120.
[11] F. Bangert, S. Grasberger, D. Kuhl, G. Meschke, Environmentally induced deterioration of concrete: physical motivation and numerical modelling, Eng. Fract. Mech. 70 (7-8) (2003) 891–910.
[12] V.H. Nguyen, B. Nedjar, J.M. Torrenti, Chemo-mechanical coupling behaviour of leached concrete. Part II: Modelling, Nucl. Eng. Des. 237 (2007) 2090–2097.
[13] C. Le Bellégo, G. Pijaudier-Cabot, B. Gérard, J.-F. Dubé, L. Molez, Coupled Mechanical and Chemical Damage in Calcium Leached Cementitious Structures, ASCE J. Eng. Mech. 129 (2003) 333–341.
[14] N. Burlion, D. Bernard, D. Chen, X-ray microtomography: application to microstructure analysis of a cementitious material during leaching process, Cem. Concr. Res. 36 (2006) 346–357.
[15] E. Schlangen, E.A.B. Koenders, K. van Breugel, Influence of internal dilation on the fracture behaviour of multi-phase materials, Eng. Fract. Mech. 74 (2007) 18–33.
[16] J.J. Chen, J.J. Thomas, H.M. Jennings, Decalcification shrinkage of cement paste, Cem. Concr. Res. 36 (2006) 801–809.
[17] D. Bernard, G.L. Vignolles, J.-M. Heintz, Synchrotron X-ray micro-tomography: a tool for porous materials evolution modelling, in: J. Baruchel, J.Y. Buffière, E. Maire, P. Merle, G. Peix (Eds.), X-ray Tomography in Materials Science, Hermès Science, Paris, 1999, pp. 177–192.
[18] D. Bernard, D. Gendron, J.M. Heintz, B. Bordère, J. Etourneau, First direct 3D visualisation of microstructural evolutions during sintering through X-ray computed microtomography, Acta Mater. 53 (2005) 121–128.
[19] E.N. Landis, E.N. Nagy, Three-dimensional work of fracture for mortar in compression, Eng. Fract. Mech. 65 (2000) 223–234.
[20] E.N. Landis, E.N. Nagy, D.T. Keane, Microstructure and fracture in three dimensions, Eng. Fract. Mech. 70 (2003) 911–925.
[21] J. Hu, P. Stroeven, X-ray absorption study of drying cement paste and mortar, Cem. Concr. Res. 33 (2003) 397–403.
[22] E.N. Landis, T. Zhang, E.N. Nagy, G. Nagy, W.R. Franklin, Cracking, damage and fracture in four dimensions, Mat. Struct. 40 (2006) 357–364.
[23] H. Elaqra, N. Godin, G. Peix, M. R'Mili, G. Fantozzi, Damage evolution analysis in mortar, during compressive loading using acoustic emission and X-ray micro-tomography: Effects of the sand/cement ratio, Cem. Concr. Res. 37 (2007) 703–713.
[24] E. Gallucci, K. Scrivener, A. Groso, M. Stampanoni, G. Margaritondo, 3D experimental investigation of the microstructure of cement pastes using synchrotron X-ray microtomography (μCT), Cem. Concr. Res. 37 (2007) 360–368.
[25] P. Trtik, P. Stähli, E.N. Landis, M. Stampanoni, J.G.M. van Mier, Microtensile testing and 3D imaging of hydrated Portland cement, FRAMCOS-6, Fracture Mechanics of Concrete and Concrete Structures, in: A. Carpinteri, P. Gambarova, G. Ferro, G. Plizzari (Eds.), Taylor & Francis Group, London, UK, 2007, pp. 1807–1814.
[26] E. Maire, L. Salvo, P. Cloetens, M. Di Michiel, Tomographie à rayons X appliquée à l'étude des matériaux in French, Tech. ing. IN 20 (2004) 1–10.
[27] S. Lu, E.N. Landis, D.T. Keane, X-ray microtomographic studies of pore structure and permeability in Portland cement concrete, Mat. Struct. 39 (2006) 611–620.
[28] F. Natterer, Numerical methods in tomography, Acta Numer. 8 (1999) 107–141.

[29] J. Bisschop, J.G.M. van Mier, Effect of aggregates on drying shrinkage microcracking in cement-based composites, Mater. Struct. 35 (2002) 453–461.
[30] T. Shiotani, J. Bisschop, J.G.M. van Mier, Temporal and spatial development of drying shrinkage cracking in cement-based materials, Eng. Fract. Mech. 70 (2003) 1509–1525.
[31] C. Carde, G. Escadeillas, R. Francois, Use of ammonium nitrate solution to simulate and accelerate the leaching of cement paste due to deionized water, Mag. Concr. Res. 49 (1997) 295–301.
[32] M.A.B. Promentilla, T. Sugiyama, T. Hitomi, N. Takeda, Quantification of tortuosity in hardened cement pastes using synchrotron-based X-ray computed microtomography, Cem. Concr. Res. 39 (2009) 548–557.
[33] F.J. Ulm, E. Lemarchand, F.H. Heukamp, Elements of chemomechanics of calcium leaching of cement-based materials at different scales, Eng. Fract. Mech. 70 (2003) 871–889.
[34] F. Camborde, C. Mariotti, F.V. Donzé, Numerical study of rock and concrete behaviour by discrete element modelling, Comput. Geotech. 27 (2000) 225–247.
[35] F.J. Ulm, J.M. Torrenti, F. Adenot, Chemoporoplasticity of calcium leaching in concrete, J. Eng. Mech.-ASCE 125 (1999) 1200–1211.
[36] G. Frantziskonis, C.S. Desai, Constitutive model with strain softening, Int. J. Solids Struct. 23 (1987) 733–750.
[37] B. Bridge, N.D. Patel, D.N. Waters, On the Elastic Constants and Structure of the Pure Inorganic Oxide Glasses, Phys. Status Solidi A 77 (1983) 655.
[38] A. Boumiz, C. Vernet, F. Cohen Tenoudji, Mechanical properties of cement pastes and mortars at early ages : evolution with time and degree of hydration, Adv. Cem. Based Mater. 3 (1996) 94–106.
[39] C.J Haecker, E.J. Garboczi, J.W. Bullard, R.B. Bohn, Z. Sun, S.P. Shah, T. Voigt, *Modeling the linear elastic properties of Portland cement paste*, Cem. Concr. Res. 35 (2005) 1948–1960.
[40] M.P. Lutz, P.J.M. Monteiro, R.W. Zimmerman, Inhomogeneous interfacial transition zone model for the bulk modulus of mortar, Cem. Concr. Res. 27 (1997) 1113–1122.
[41] C.C. Yang, Effect of the transition zone on the elastic moduli of mortar, Cem. Concr. Res. 28 (1998) 727–736.
[42] Z. Hashin, P.J.M. Monteiro, An inverse method to determine the elastic properties of the interphase between the aggregate and the cement paste, Cem. Concr. Res. 32 (2002) 1291–1300.
[43] F.H. Heukamp, F.J. Ulm, J.T. Germaine, Does calcium leaching increase ductility of cementitious materials? Evidence from direct tensile tests, J. Mater. Civ. Eng. 17 (2005) 307–312.
[44] N. Hearn, Effect of shrinkage and load-induced cracking on water permeability of concrete, ACI Mater. J. 96 (1999) 234–241.
[45] F.H. Heukamp, E. Lemarchand, F.J. Ulm, The effect of interfacial properties on the cohesion of highly filledcomposite materials, Int. J.Solids Struct. 42 (2005) 287–305.
[46] D. Chen, I. Yurtdas, N. Burlion, J.F. Shao, Elastoplastic damage behaviour of a mortar subjected to compression and desiccation, ASCE J. Eng. Mech. 133 (2006) 464–472.